Detectors

17.11.20

General schedule

- ⋆ History
- ⋆ Introduction to general relativity
- ⋆ Detection principles
- ⋆ Detectors
  - ⋆ Sensitivity curve,
  - ⋆ Noise sources,
  - ⋆ Antenna patterns, triangulation.
- ⋆ Binary black-hole system
- ⋆ Bursts and continuous waves
- ⋆ Rates and populations, stochastic GW background, cosmology
- ⋆ Testing general relativity
- ⋆ Data analysis: waveforms and detection
- ⋆ Data analysis: parameter estimation

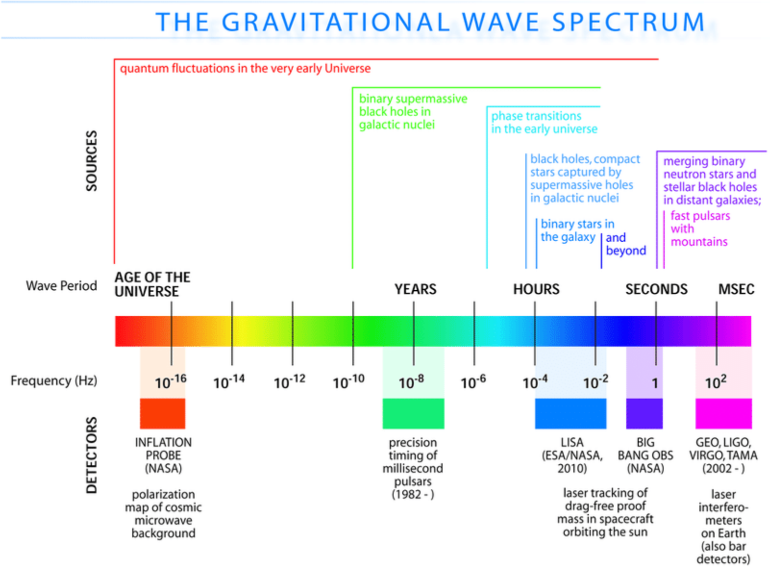
THE GRAVITATIONAL WAVE SPECTRUM
SOURCES
quantum fluctuations in the very early Universe
binary supermassive black holes in galactic nuclei
phase transitions in the early universe
black holes, compact stars captured by supermassive holes in galactic nuclei
binary stars in the galaxy
and beyond
merging binary neutron stars and stellar black holes in distant galaxies;
fast pulsars with mountains
Wave Period
AGE OF THE UNIVERSE
YEARS
HOURS
SECONDS
MSEC
Frequency (Hz)
10^{-16}
10^{-14}
10^{-12}
10^{-10}
10^{-8}
10^{-6}
10^{-4}
10^{-2}
1
10^{2}
DETECTORS
INFLATION PROBE (NASA)
polarization map of cosmic microwave background
precision timing of millisecond pulsars (1982 -)
LISA (ESA/NASA, 2010)
BIG BANG OBS (NASA)
laser tracking of drag-free proof mass in spacecraft orbiting the sun
GEO, LIGO, VIRGO, TAMA (2002 -)
laser interfero-meters on Earth (also bar detectors)

Detection principle: laser interferometry

"How to measure distance when the ruler also changes length?"

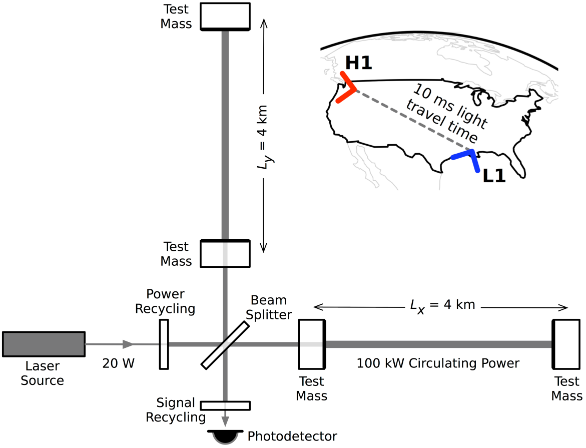

Changes in arms length are **very** small: $\delta L_x - \delta L_y = \Delta L < 10^{-18}$ m (smaller than the size of the proton). Wave amplitude $h = \Delta L / L \leq 10^{-21}$.

Change of arms' length $\leftrightarrow$ variation in light travel time

Change of the x-arm: $ds^2 = -c^2 dt^2 + (1 + h_{xx})\, dx^2 = 0.$

Assume $h(t)$ is constant during light's travel through interferometer, replace $\sqrt{1 + h_{xx}}$ with $1 + h_{xx}/2$, integrate from $x = 0$ to $x = L$:

$$\int dt = \frac{1}{c} \int \left(1 + \frac{1}{2} h_{xx}\right) dx \quad \to \quad t_x = h_{xx} L / 2c.$$

Round-trip time in the x-arm: $t_x = h_{xx} L / c.$

Round-trip time in the y-arm: $t_y = -hL/c \qquad (h_{yy} = -h_{xx} = -h)$

Round-trip times difference: $\boxed{\Delta\tau = 2hL/c}$

Phase difference (dividing $\Delta\tau$ by the radian period of light $2\pi/\lambda$):

$$\boxed{\Delta\phi = \frac{4\pi}{\lambda} hL}.$$

Orders of magnitude comparison

- ⋆ GW150914: $h = \Delta L/L \simeq 10^{-21}$
- ⋆ Two neutron stars merging near Sgr A*: $\sim 10^{-19}$
- ⋆ Io orbiting Jupiter: $\sim 3 \times 10^{-25}$
- ⋆ Hulse-Taylor pulsar: $\sim 10^{-26}$
- ⋆ Dumbbell 1 tonnes masses, 1 m arm from 300 m: $\sim 10^{-35}$
- ⋆ Collision of two aircraft carriers: 5×10^{-46}
- ⋆ Angry protester shaking her fist: $\sim 7 \times 10^{-52}$
- ⋆ Tennis ball rotating on 1 m string, from 10 m: $\sim 10^{-54}$.

- ⋆ The amplitude $h = \Delta L/L \leq 10^{-21}$ corresponds to the distance measurement between Earth and Sun with the accuracy of the size of the atom (10^{-10} m)
- ⋆ Ground motion amplitude near the detector: $\Delta L \sim 10^{-6}$ m ($10^{12} \times h$)
- ⋆ Laser wavelength: 10^{-6} m ($10^{12} \times h$)

Initial estimates

For a spherical wave of amplitude $h(r)$,

- $\star$ flux of energy is $F(r) \propto h^2(r)$,
- $\star$ the luminosity $L(r) \propto 4\pi r^2 h^2(r)$.

Conservation of energy (flux through surface at r):

$$\implies h(r) \propto 1/r.$$

Radiating modes: quadrupole and higher

For a mass distribution $\rho(r)$, conserved moments:

- $\star$ monopole $\int \rho(r) d^3 r$ - total mass-energy (energy conservation),
- $\star$ dipole $\int \rho(r) r d^3 r$ - center of mass-energy (momentum conservation).

Sensitivity $\rightarrow$ amplitude $\rightarrow$ volume

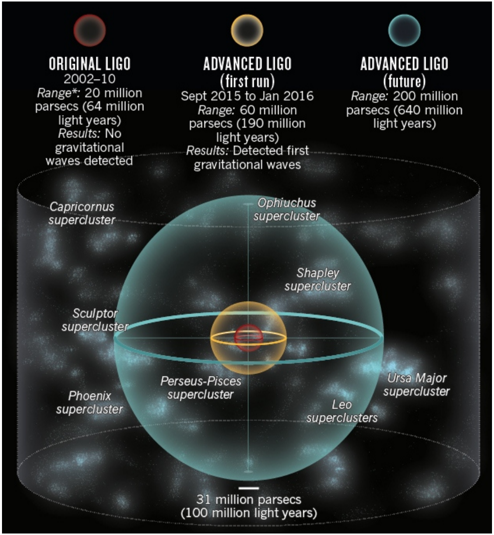

- $\star$ Detector's sensitivity (registering waves of amplitude h) is related to maximal range r, $h \propto 1/r$
- $\star$ Reachable cosmic volume $V \propto r^3$
- $\star$ Increase of sensitivity $h \rightarrow 0.1h$ gives $r \rightarrow 10r$, that is $V \rightarrow 1000V$.

How the sensitivity curve looks like?

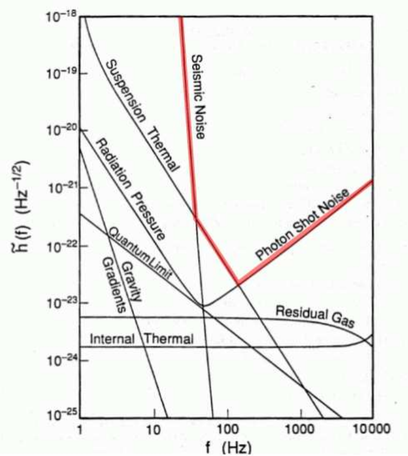

Initial LIGO proposal (1989)

⋆ Range of frequencies similar to sensitivity of our hearing:

From 20 Hz (H0) to a few thousands Hz (3960 Hz, H7) - 8 octaves,

⋆ Poor, like for an ear, angular resolution (directional capabilities).

Advanced LIGO design sensitivity

GW interferometers are noise-dominated detectors!

Sensitivity - amplitude spectral density of the noise

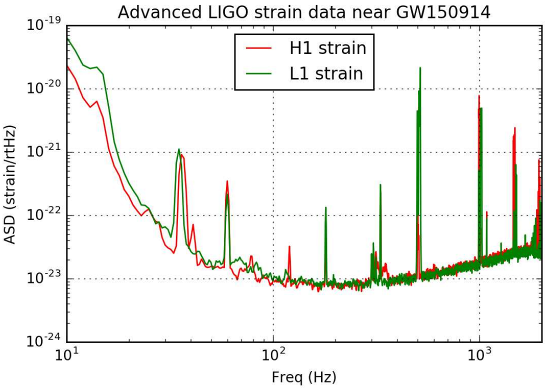

- ⋆ *Plot dominated by instrumental noise, lines*: mirror suspension resonances at 500 Hz and harmonics, calibration lines and power lines (60 Hz and harmonics) etc.,
- ⋆ Data sampled at 16384 Hz, so the Nyquist frequency is 8192 Hz,
- ⋆ Data stream: ∼50 MB/s (main GW + auxiliary ”witness” channels).

Sensitivity - amplitude spectral density of the noise

- ⋆ GW detectors register time series $x(t)$ (as light phase difference at the photodiode),
- ⋆ The average power P of $x(t)$ over T:

$$P = \lim_{T\to\infty} \frac{1}{T} \int_{-\infty}^{\infty} |x(t)|^2 dt = \lim_{T\to\infty} \frac{1}{T} \int_{-\infty}^{\infty} |\hat{x}(f)|^2 df$$

$$\text{Parseval's theorem:} \quad \int_{-\infty}^{\infty} |x(t)|^2 dt = \int_{-\infty}^{\infty} |\hat{x}(f)|^2 df,$$

with $\hat{x}(f)$ the Fourier transform of $x(t)$.

- ⋆ Power spectral density (PSD) is

$$S(f) = \lim_{T\to\infty} \frac{1}{T} |\hat{x}(f)|^2, \quad \text{units: W/Hz.}$$

- ⋆ Amplitude spectral density (ASD) is

$$S_{ASD}(f) = \sqrt{S(f)}, \quad \text{units: } \sqrt{\text{W/Hz}}.$$

For a dimensionless amplitude $h = \Delta L/L$, the amplitude spectral density has units of $1/\sqrt{Hz}$.

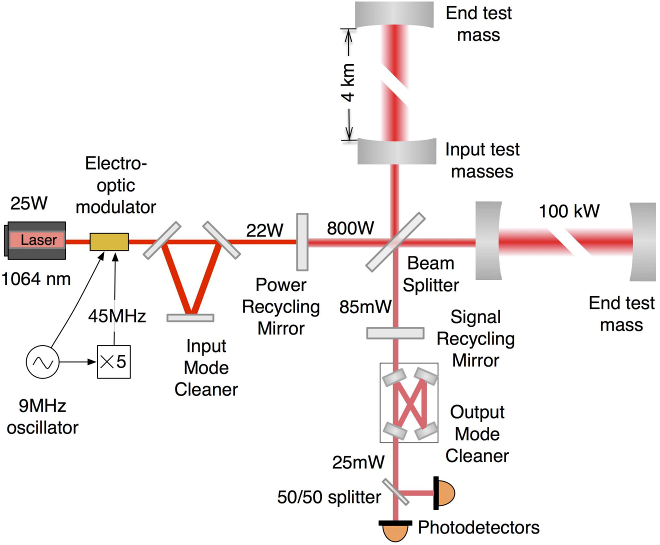
End test mass
4 km
Input test masses
Electro-optic modulator
25W
Laser
1064 nm
45MHz
×5
9MHz oscillator
22W
800W
100 kW
Power Recycling Mirror
Input Mode Cleaner
Beam Splitter
End test mass
85mW
Signal Recycling Mirror
Output Mode Cleaner
25mW
50/50 splitter
Photodetectors

Delay line vs Fabry-Perot

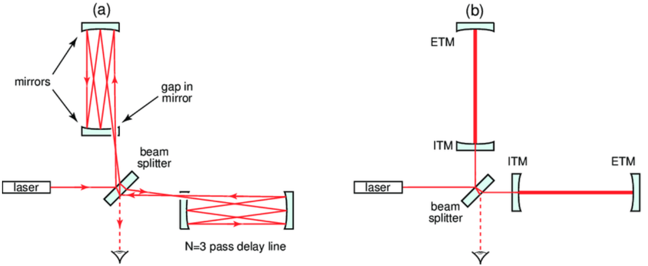

- ⋆ Key point for GW detection is light path folding: making the light storage time higher without extending the interferometer,
- ⋆ Charles Fabry, Alfred Perot (1899) resonance cavity: standing wave, storage for $\approx$5 ms, corresponding to $\sim$ 400 round trips.

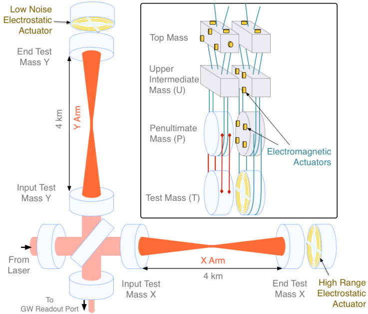

Seismic noise

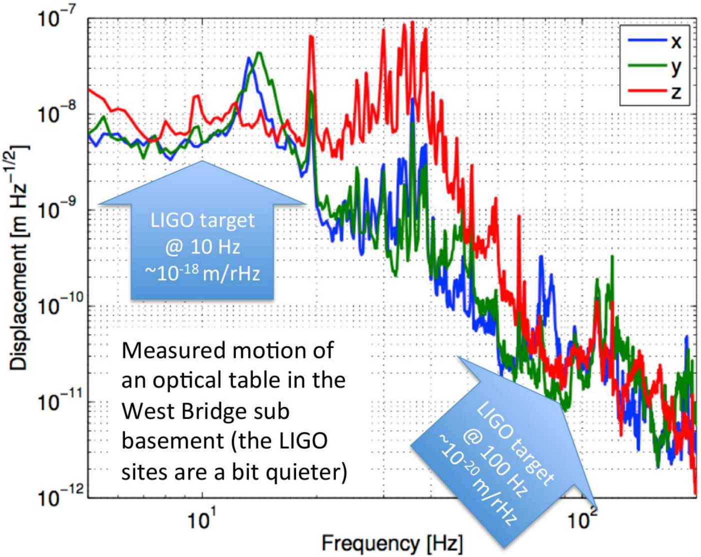

Isolation from seismic noise

Pendulum: above the resonant frequency (1 Hz) the motion of mass is smaller than the motion of suspension point (at 10 Hz - factor 10^2). LIGO, Virgo: multiply suspended pendula.

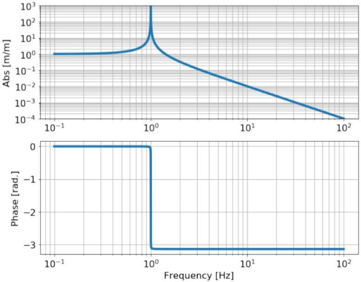

Fresco by Luigi Sabatelli (1772-1850)

Isolation from seismic noise

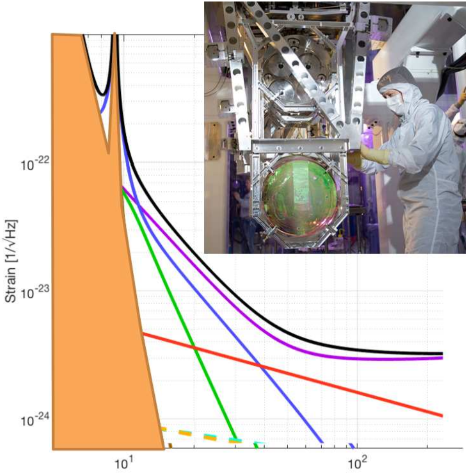

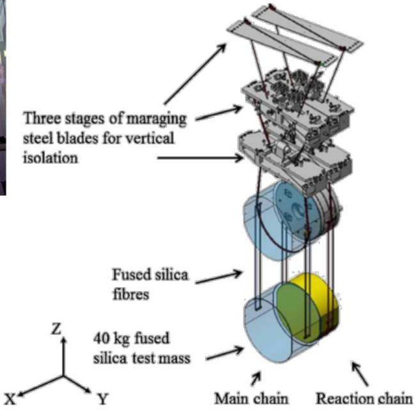

Newtonian noise

Ground and air around the mirror (test mass) moves, exerting Newtonian ($F = -GMm/r^2$) gravitational force.

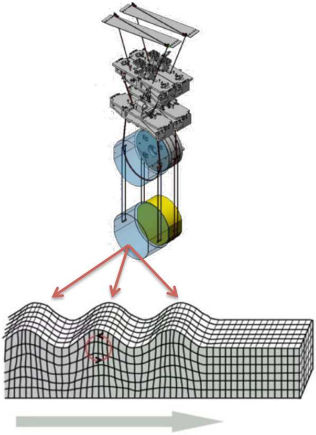

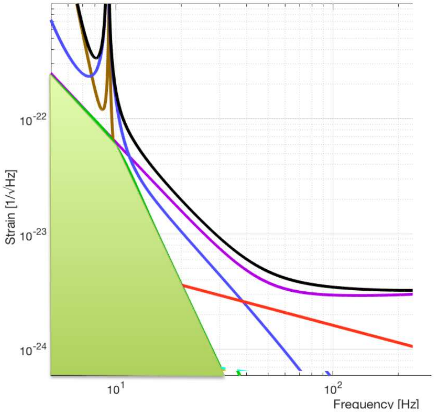

Thermal/brownian noise, mirror coatings

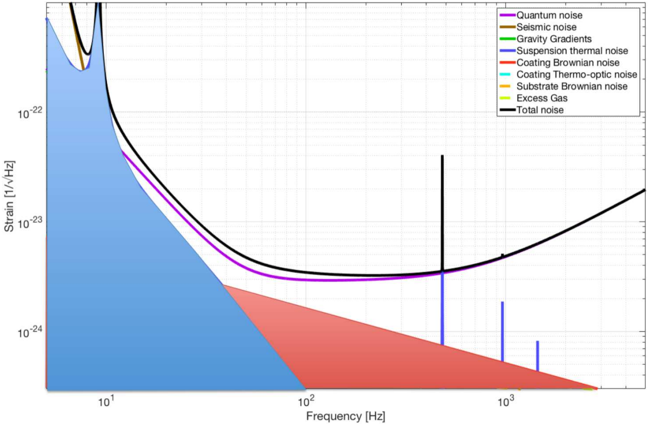

- ⋆ Test masses (mirrors and coating) are at finite temperature (LIGO, Virgo - not a KAGRA) → thermodynamical fluctuations of mechanical and optical variables, coupling with the environment (thermal energy ($k_B T$) populates the oscillatory levels of the instrument),
- ⋆ Friction and dissipation losses determine how much energy exchanged with the environment.

Mirror coatings

- Alternate layers of high and low refractive index materials

Material	Refractive index	Loss angle
Silica SiO_2	1.45	0.4×10^{-4}
Tantala Ta_2O_5	2.03	3.4×10^{-4}
Titania-doped tantala Ta_2O_5-TiO_2	2.07	**2.3×10^{-4}**

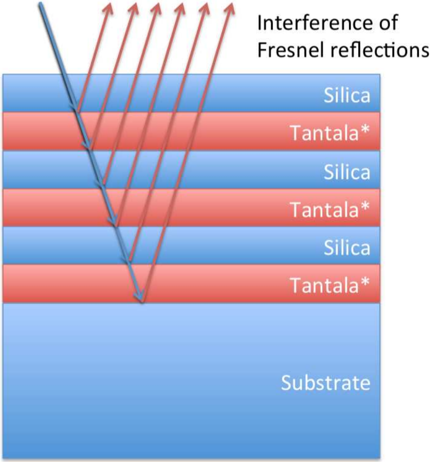

* Titania doped

The effective loss angle is a combination of those of the two materials: dominated by the high index material

Suspension thermal noise

High Q material (Q factor - measuring how damped a resonator is) e.g. silica or sapphire, minimizes dissipation: test masses (mirrors), and also suspension wires made of the same high Q materials.

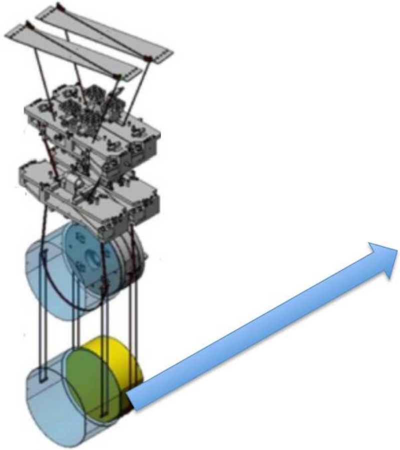

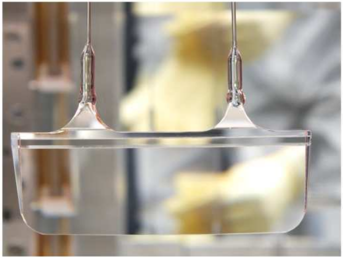

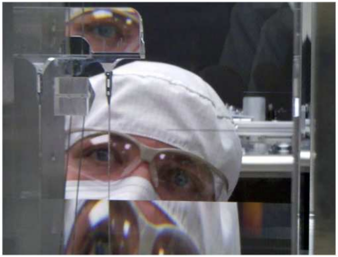

Radiation pressure and quantum shot noise

- ⋆ Shot noise: uncertainty in intensity due to photon counting statistics ($\sim 1/\sqrt{P}$),
- ⋆ Radiation pressure noise: quantum limited intensity fluctuations (photons exert a time varying force, $\sim\sqrt{P}/m$)
- ⋆ The problem - optimization of the quadrature sum $\sqrt{h_{sn}^2 + h_{rp}^2}$,

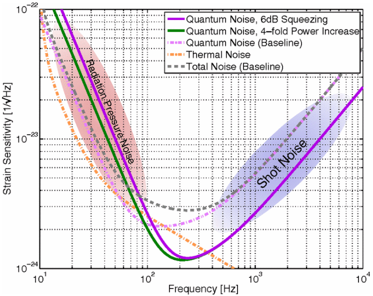

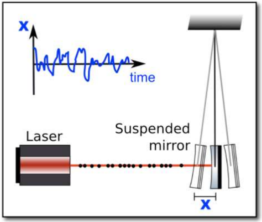

wavelength

$$h_{\rm sn}(f) = \frac{1}{L}\sqrt{\frac{\hbar c\lambda}{2\pi P}}$$

optical power

Mirror mass Arm length

$$h_{\rm rp}(f) = \frac{1}{mf^2L}\sqrt{\frac{\hbar P}{2\pi^3 c\lambda}}$$

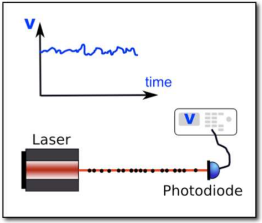

photon radiation pressure noise S. Hild **photon shot noise**

Antenna directionality

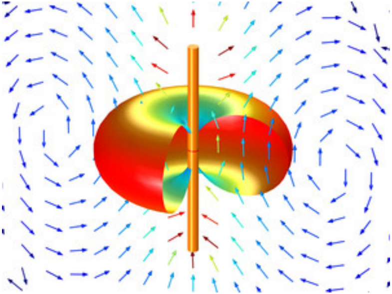

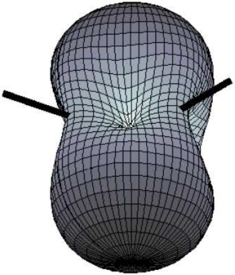

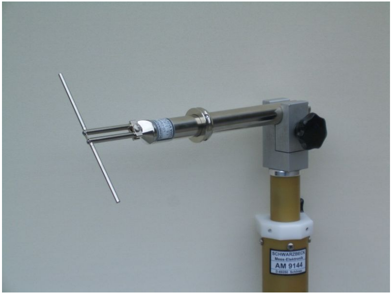

Antenna patterns (antenna characteristics)

The detector response is

$$\frac{\Delta L}{L} = F_+ h_+ + F_\times h_\times ,$$

where F_+ and $F_\times$ are

$$\begin{aligned} F_+ &= \frac{1}{2}(1+\cos^2\theta)\cos 2\phi \cos 2\psi \\ &+ \cos\theta \sin 2\phi \sin 2\psi, \\ F_\times &= \frac{1}{2}(1+\cos^2\theta)\cos 2\phi \sin 2\psi \\ &+ \cos\theta \sin 2\phi \cos 2\psi \end{aligned}$$

(see e.g. Drew Keppel PhD, `thesis.library.caltech.edu/1901`, Chap. 3)

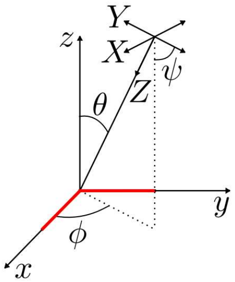

Euler angles $\{\phi, \theta, \psi\}$ used in converting from the GW propagation frame {X, Y, Z} to the detector frame {x, y, z}

Taking into account a second angle related to the source orientation, ι (inclination between the orbital plane and direction towards the detector):

$$h(t) = h_+(t)F_+(1+\cos^2\iota) + h_\times(t)F_\times(2\cos\iota)$$

Antenna patterns (antenna characteristics)

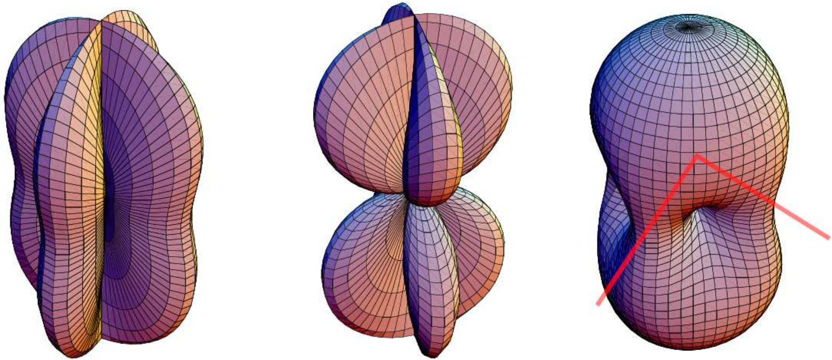

Antenna patterns for interferometer detectors for $+$ (left), $\times$ (center), and combined (right) polarizations with polarization angle $\psi = 0$.

Global detector network: LIGO-Virgo-(KAGRA)

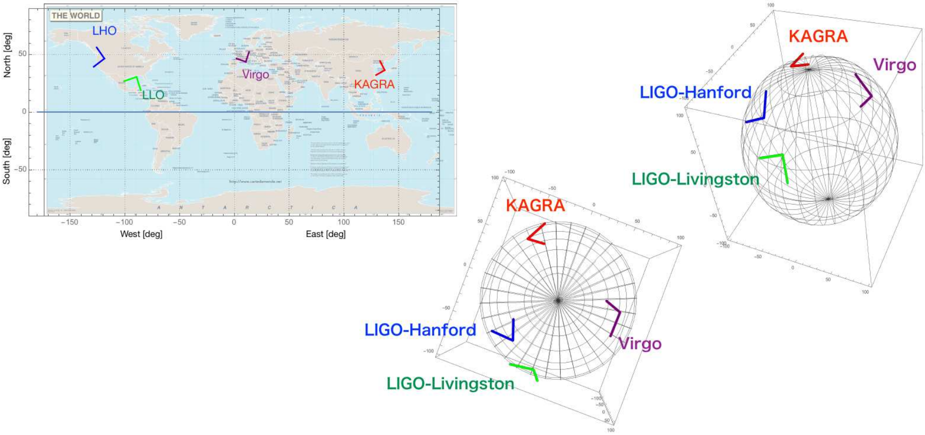

Light travel time between Livingston-Hanford: 10 ms, Hanford-Virgo: 27 ms, Livingston-Virgo: 26 ms.

Antenna pattern of the network of GW detectors

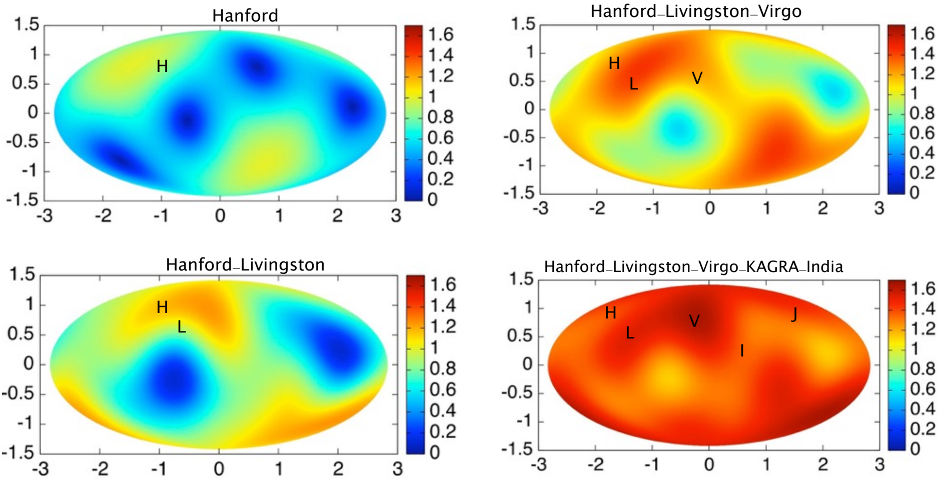

Network of detectors: sky position/triangulation

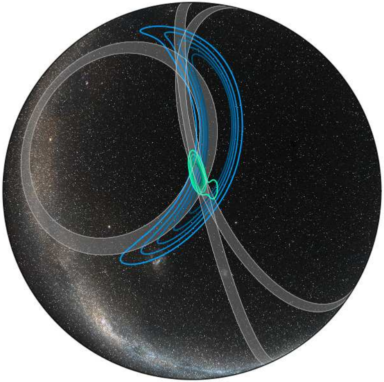

Credit: LIGO/Virgo/NASA/Leo Singer (Milky Way image: Axel Mellinger)

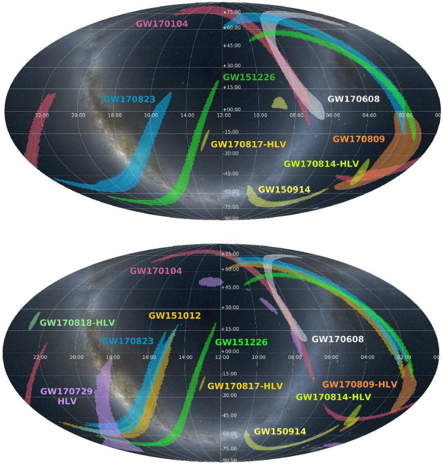

GW170814

Top: initial results, bottom: refined using updated calibration and waveform models.

Sky localization via triangulation

Triangulation uses time delays between detectors. Single-site timing accuracy is approximately

$$\sigma_t = \frac{1}{2\pi\rho\sigma_f} \approx 10^{-4}\, s \approx 1/100 \text{ light travel time},$$

with the SNR ρ for a given detector and σ_f effective bandwidth of the signal (typically 100 Hz).

In real observations, one takes also into account:

- ⋆ signal phase and amplitude consistency between detectors,
- ⋆ uncertainty in the emitted gravitational waveform,
- ⋆ instrumental calibration accuracies (timing accuracies ∼5 ms).

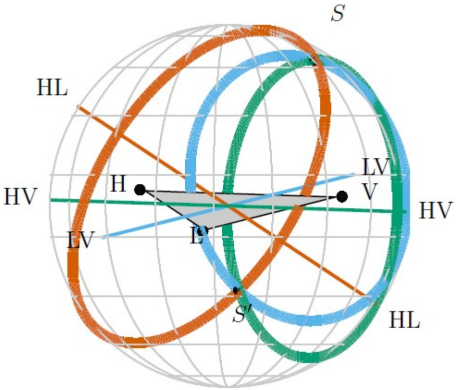

Three detectors (L, H, V) marked by black dots. The locus of constant time delay (with associated timing uncertainty) between two detectors forms an annulus on the sky concentric about the baseline between the two sites (labeled by the two detectors). For three detectors, these annuli may intersect in two locations: true source direction (S) and S', a mirror image with respect to the plane passing through the three sites.
For four or more detectors there is a unique intersection region.

Sky localization: number of detectors

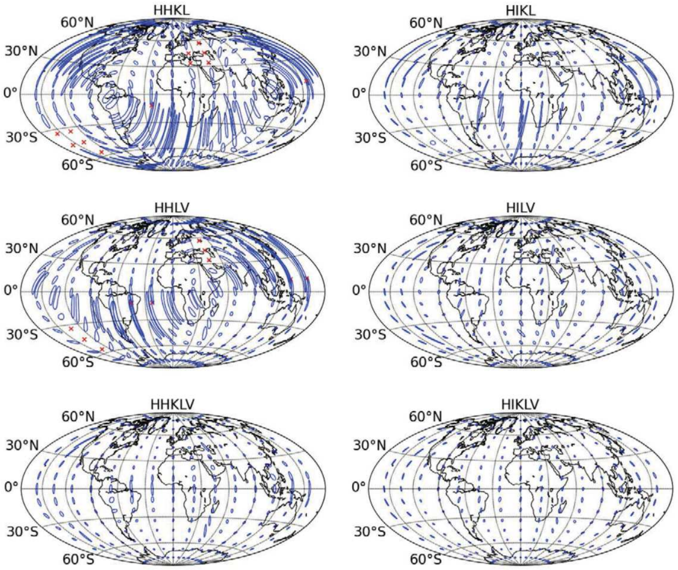

S Fairhurst 2014 J. Phys.: Conf. Ser. 484 012007

Literature

- ⋆ Drew Keppel PhD, thesis.library.caltech.edu/1901,
- ⋆ "Prospects for observing and localizing gravitational-wave transients with Advanced LIGO, Advanced Virgo and KAGRA", link.springer.com/article/10.1007/s41114-020-00026-9,
- ⋆ "Gravitational Wave Detection by Interferometry (Ground and Space)", M. Pitkin, S. Reid, S. Rowan, J. Hough, link.springer.com/article/10.12942/lrr-2011-5
- ⋆ "Gravitational-wave sensitivity curves", C. Moore, R. Cole, C. Berry, arXiv:1408.0740,
- ⋆ "Spacetime Quest", www.laserlabs.org/spacetimequest.php (documentation: www.laserlabs.org/downloads/SpacePyQuest.pdf),
- ⋆ Minecraft LIGO: minecraft.ozgrav.org:25593